J|A|C|S ARTICLES

Published on Web 08/05/2009

Mass-Produced Nanogap Sensor Arrays for Ultrasensitive Detection of DNA

Somenath Roy, Xiaojun Chen, Mo-Huang Li, Yanfen Peng, Franklin Anariba, and Zhiqiang Gao*

Institute of Bioengineering and Nanotechnology, 31 Biopolis Way, Singapore 138669

Received March 11, 2009; E-mail: zqgao@ibn.a-star.edu.sg

Abstract: In this report, an electrical detection scheme for the quantification of DNA using a nanogap sensor array is detailed. The prime objective is to develop a novel sensing procedure, based on the electronic transduction mechanism, which would mitigate the problems intrinsic to nanostructure-based biosensing devices. Design considerations of the sensor array take into account the feasibility of mass production in a cost-effective way by using standard silicon microfabrication technologies. The sensing mechanism relies on bridging the nanogap upon hybridization of the two termini of a target DNA with two different surface-bound capture probes, followed by a simple metallization step. About 2 orders of magnitude enhancement in conductance, as referred to a clean background (<1.0 pS) observed at a control sensor, was obtained in the presence of as little as 1.0 fM target DNA. This sensitivity is comparable to the best of electrochemical/electrical biosensors. A linear relationship between the conductance and the DNA concentration was obtained from 1.0 fM to 1.0 pM with an exceptional signal intensity of 2.1×10^4% change per unit concentration. This change in conductivity is so large that it can unambiguously detect the concentration of DNA quantitatively and may obviate the need for target amplification used in current DNA tests. Moreover, the sensor array exhibited excellent single-base mismatch discrimination due to its unique vertically aligned nanostructure and the two-probe configuration.

Introduction

With the advent of DNA microarrays, the past decade witnessed a paradigm shift in gene expression profiling and single nucleotide polymorphism (SNP) detection.[1,2] Microarray technology, in conjunction with polymerase chain reactions (PCR), has become the state-of-the-art owing to its massive parallelism and high throughput. In spite of exhibiting considerable promises to the development of molecular biology and medicine, the fluorescence-based microarray technique suffers from some inherent shortcomings in optical detections, including the need for expensive and bulky optical scanners, potential image corruption from photobleaching of fluorescence dyes, and ambiguous readout due to spectral cross-talk between tagging fluorescence dyes.[3] Electronic analogues of the DNA microarray could offer a viable alternative for the rapid quantification of DNA, which is especially desirable for clinical and defense applications.

In the past few years, researchers have proposed several labeled and label-free sensing technologies that feature direct electronic transduction. The direct electrical transduction has several advantages with respect to other approaches. One of the most promising is the feasibility for on-chip integration of sensor units with an allied signal processing circuitry, using standard complementary metal oxide semiconductor (CMOS) technology. Referring to the literature, field-effect, resistive, and capacitive devices have been investigated more widely, using various micro- and nanofabrication techniques.[4−8] On the other hand, the combination of CMOS technology and enzymatic amplification has provided a unique opportunity of fabricating high density electrochemical/electrical biosensor arrays.[9−12] For example, CombiMatrix Corporation has developed a DNA array with up to 12 000 individual sensors, fabricated using the CMOS compatible microfabrication technology, although the subpicomolar detection limit is not as impressive as its density.[11] Later,

(1) Schena, M.; Shalon, D.; Davis, R. W.; Brown, P. O. *Science* **1995**, *270*, 467–470.
(2) Lashkari, D. A.; DeRisi, J. L.; McCusker, J. H.; Namath, A. F.; Gentile, C.; Hwang, S. Y.; Brown, P. O.; Davis, R. W. *Proc. Natl. Acad. Sci. U.S.A.* **1997**, *94*, 13057–13062.
(3) Lewis, E. K.; Haaland, W. C.; Nguyen, F. D.; Heller, A.; Allen, M. J.; MacGregor, R. R.; Berger, C. S.; Willingham, B.; Burns, L. A.; Scott, G. B. I.; Kittrell, C.; Johnson, B. R.; Curl, R. F.; Metzker, M. L. *Proc. Natl. Acad. Sci. U.S.A.* **2005**, *102*, 5346–5351.
(4) Fritz, J.; Cooper, E. B.; Gaudet, S.; Sorger, P. K.; Manalis, S. R. *Proc. Natl. Acad. Sci. U.S.A.* **2002**, *99*, 14142–14146.
(5) Hahm, J.; Lieber, C. M. *Nano Lett.* **2004**, *4*, 51–54.
(6) Milovic, N.; Behr, M. J.; Godin, R. M.; Chih-Sheng, J. H.; Kristofor, R. P.; Chandrasekaran, A.; Peter, R. R.; Sasisekharan, R.; Manalis, S. R. *Proc. Natl. Acad. Sci. U.S.A.* **2006**, *103*, 13374–13379.
(7) Star, A.; Tu, E.; Niemann, J.; Gabriel, J. C. P.; Joiner, C. S.; Valcke, C. *Proc. Natl. Acad. Sci. U.S.A.* **2006**, *103*, 921–926.
(8) Uslu, F.; Ingebrandt, S.; Mayer, D.; Bocker-Meffert, S.; Odenthal, M.; Offenhausser, A. *Biosens. Bioelectron.* **2004**, *19*, 1723–1731.
(9) Sassolas, A.; Leca-Bouvier, B. D.; Blum, L. *Chem. Rev.* **2008**, *108*, 109–139.
(10) Roy, S.; Gao, Z. *Nano Today* **2009**, *4* (4), 318–334.
(11) Liu, R. H.; Nguyen, T.; Schwarzkopf, K.; Fuji, H. S.; Petrova, A.; Siuda, T.; Peyvan, K.; Bizak, M.; Danley, D.; McShea, A. *Anal. Chem.* **2006**, *78*, 1980–1986.
(12) Liu, R. H.; Lodes, M. J.; Nguyen, T.; Siuda, T.; Slota, M.; Fuji, H. S.; McShea, A. *Anal. Chem.* **2006**, *78*, 4184–4193.

this DNA array was successfully applied in identifying and sequencing Influenza A virus with the help of PCR amplification.[12]

Moreover, nanogap-based biosensors have also been proposed to ultrasensitive detection of DNA. One of the early reports was from Choi's group at UC Berkeley.[13] The nanogap was fabricated in which two poly silicon electrodes were separated from each other by a 50 nm gap. Because of the lack of rigidity, the immobilized oligonucleotides are randomly tangled, whereas a specific conformation is assumed when they hybridize with complementary DNA strands. The difference in geometric structure associated with a change in counterion concentration upon hybridization leads to a change in the capacitance of the nanogap. Unfortunately, no concentration information is available in this report. It is more a mechanistic study than a DNA sensor development. Another report on the application of the nanogap in DNA sensing, relying on the native charge transport through the double helix, was published by Hashioka and coworkers.[14] A 40 nm gap was fabricated between a gold and a titanium electrode using conventional photolithography followed by the oxidation of the titanium and stripping of the titanium oxide. A current increment of ~19 nA at 1 V bias was observed after incubating with 1.0 μM thiolated target DNA. Later, the detection of DNA based on its native charge transport was also investigated by Shiigi et al.[15] They constructed a film of gold nanoparticles (GNP), with decanedithiol as a spacer, between platinum microelectrodes. In their approach, the authors monitored the tunneling of charge carriers before and after the formation of the capture probe−target DNA duplex, bridging the adjacent GNPs. Since the flow of charge carriers through a DNA molecule is rather limited, the change in the baseline electrical current upon hybridization of 100 μM target single-stranded DNA (ss-DNA) was less than 1%, making this approach prone to yield false signals. In another effort, Roy et al. exploited a ss-DNA sandwiched between a pair of carbon nanotube electrodes to probe into its native charge conductivity of the ss-DNA as well as its hybridized duplex.[16] Because of the presence of very short chemical linkers between the carbon nanotube electrodes and the capture probes, the signal-to-noise ratio was enhanced to 25%.[16] Although interesting for fundamental understanding of the charge flow mechanism, the reliability of signal from such a single nanotube−single DNA system may not be high enough to be accepted in the biomedical community.

Furthermore, to cover both short (<300 bp) and long genes, a nanogap of ~10 nm is required. The ability to affordably and efficiently fabricate such highly uniformed nanogap structures with high scale-up potentials is important to many technical applications, and yet, it remains a technical challenge.[17−23] Most of the bottom-up approaches suffer from certain limitations such as device-to-device uniformity, reflecting the variations in the device fabrication processes, low yield, and low scalability.[17] On the other hand, the widely used top-down approaches for fabricating narrow nanogaps, such as mechanical break junction,[18] electron beam lithography,[19] electromigration,[20] dip-pen lithography,[21] transmission electron microscope-assisted nanosputtering,[22] and electroplating,[23] have to resolve issues such as high cost and low yield in order to be one step closer to routine fabrications.

In this work, we addressed the aforementioned issues of device homogeneity and signal reliability by implementing a mass-producible fabrication technique along with a novel sensing protocol that can accurately detect the target DNA at extremely low concentrations. Instead of a label-free procedure for electrically bridging the nanogap by the intrinsically insulating target DNA, we appended a DNA-templated silver nanowire formation along the hybridized DNA strands step in our detection scheme, enabling a much more sensitive electrical detection with minimal background and with enhanced mismatch discrimination.

Experimental Section

Reagents. Thiol-terminated DNA capture probes used in this work were custom-made by Sigma-Genosys (Woodlands, TX) and used as received. Other oligonucleotides were from 1st Base Pte Ltd. (Singapore). All other reagents were purchased from Sigma-Aldrich (St. Louis, MO) and used without further purification. To remove any organic residue or remnant photoresist, the devices were first cleaned in Nanostrip[24] solution for 15 min, thoroughly rinsed with deionized (DI) water, and dried in a stream of nitrogen.

Fabrication of Nano-MIM Devices. Metal/insulator/metal multilayer (hereinafter abbreviated as "nano-MIM") devices were fabricated on 4 in. silicon wafers (coated with 500 nm SiO_2) using standard photolithography techniques (Figure 1). Well-defined sidewalls of the insulating layer and the top electrode, necessary for molecular bridging, were patterned by two different methods: (i) reactive ion etching (RIE) and (ii) photolithography-liftoff processes. The RIE process resulted in a much better definition of the sidewalls. Therefore, it was employed in the fabrication process. Plasma enhanced chemical vapor deposition (PECVD) was used to deposit a SiO_2 insulating layer. After realizing the bottom electrode, a 5−20 nm SiO_2 insulating layer was deposited on the entire wafer by the PECVD method using tetraethoxyorthosilicate (TEOS) vapor as a source for silicon and O_2 as precursor gas. Since the morphology and electrical properties of the SiO_2 insulating layer play a pivotal role in the performance of the nano-MIM sensors, several optimization experiments were performed to obtain a very compact and homogeneous SiO_2 layer. A 45 s deposition time with O_2 and TEOS vapor flow rates of 2000 sccm and 0.5 L/min, respectively, at a chamber pressure of 850 mTorr, gave us the best results. By ellipsometric measurements, we determined that, under the optimized conditions, there was only <0.5 nm variation in the SiO_2 layer thickness over the entire 4 in. substrate (Figure S1 in the Supporting Information). A standard photolithography process was then performed to pattern the top electrode followed by a RF magnetron sputtering of Au (150 nm) on a Ti (15 nm) adhesion layer. After lift-off, the wafer was placed in a RIE chamber for selective and complete removal of the SiO_2 layer from the undesired portion of the bottom electrode. In this case, the top metal layer stack acted as a well-defined mask for etching the SiO_2 layer, and

(13) Choi, Y. K.; Lee, J. S.; Zhu, J.; Somorjai, G. A.; Lee, P. K.; Bokor, J. *J. Vac. Sci. Technol. B* **2003**, *21*, 2951–2955.
(14) Hashioka, S.; Saito, M.; Tamiya, E.; Matsumura, H. *Appl. Phys. Lett.* **2004**, *85*, 687–689.
(15) Shiigi, H.; Tokonami, S.; Yakabe, H.; Nagaoka, T. *J. Am. Chem. Soc.* **2005**, *127*, 3280–3281.
(16) Roy, S.; Vedala, H.; Roy, A. D.; Kim, D. H.; Doud, M.; Mathee, K.; Shin, H. K.; Shimamoto, N.; Prasad, V.; Choi, W. *Nano Lett.* **2008**, *8*, 26–30.
(17) Teo, B. K.; Sun, X. H. *Chem. Rev.* **2007**, *107*, 1454–1532.
(18) Reed, M. A.; Zhou, C.; Muller, J.; Burgin, T. P.; Tour, J. M. *Science* **1997**, *278*, 252–254.
(19) Liu, K.; Avouris, P.; Bucchigna, J.; Martel, R.; Sun, S.; Michl, J. *Appl. Phys. Lett.* **2002**, *80*, 865–867.
(20) Park, H.; Alivisatos, A. P.; McEuen, P. L. *Appl. Phys. Lett.* **1999**, *75*, 301–303.
(21) Zhang, H.; Chung, S. W.; Mirkin, C. A. *Nano Lett.* **2003**, *3*, 43–45.
(22) Fischbein, M. D.; Drndic, M. *Nano Lett.* **2007**, *7*, 1329–1337.
(23) Morpurgo, A. F.; Marcus, C. M.; Robinson, D. B. *Appl. Phys. Lett.* **1999**, *74*, 2084–2086.
(24) Nanostrip solution is a mixture of H_2SO_4, H_2SO_5, H_2O_2, and water, available commercially from Cyantek Corporation.

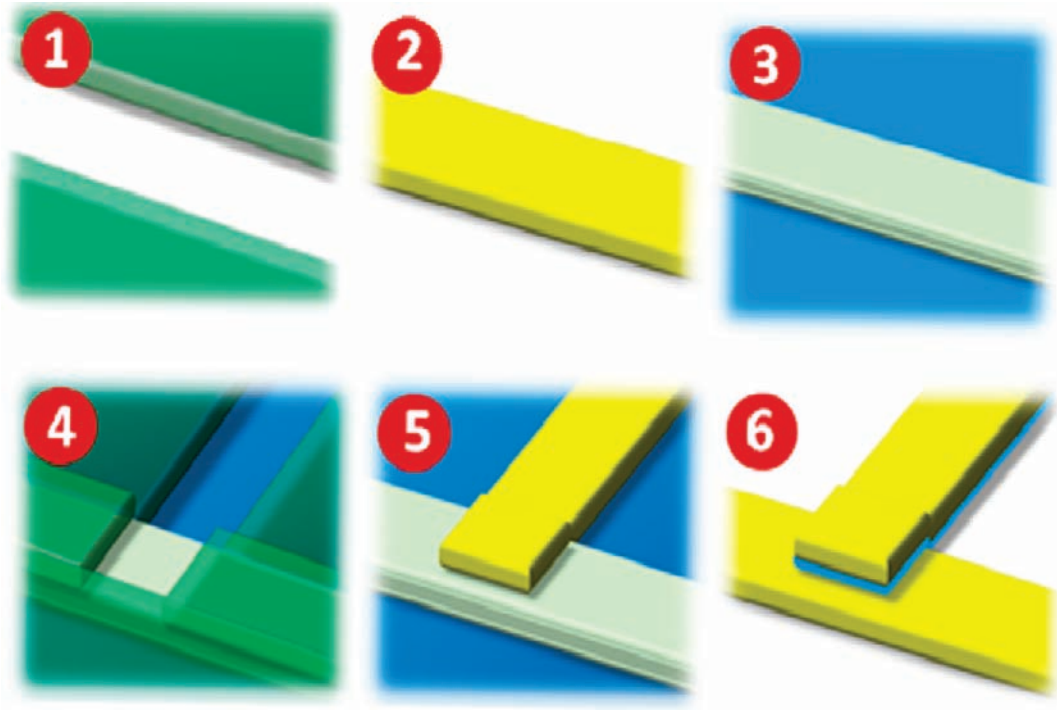

Figure 1. Process flow for the fabrication of the nano-MIM structure: (1) patterning bottom electrode on a SiO_2-coated silicon wafer by photolithography; (2) Ti/Au deposition and lift-off; (3) SiO_2 deposition on the whole wafer by PECVD; (4) patterning top electrode by photolithography; (5) Ti/Au deposition and lift-off; (6) RIE of SiO_2 from the surface of the bottom electrode.

microscopic observation suggested that reasonably sharp edges and smooth gold surfaces were obtained (Figure S2 in the Supporting Information). Good nano-MIM structures with the SiO_2 insulating layer as thin as 5 nm can easily be fabricated through adjusting experimental variables in the SiO_2 deposition process.

Capture Probe Immobilization. The current approach involves two sets of capture probes with different sequences. The 5′ forward capture probe (CP1) was a 21-base oligonucleotide with a spacer length of 9 bases, while the 3′ reverse capture probe (CP2) was also a 21-base oligonucleotide.[22] With these probes, a full-length human protein kinase B-2 (PKB2, 1446 bp) could be detected as the model target DNA (Supporting Information). The characteristics of both capture probes are unique for PKB2, and the probes hybridize to the 5′ and 3′ ends of PKB2, respectively. In brief, a freshly cleaned device was incubated in phosphate-buffered saline (PBS:10 mM phosphate buffer, 139 mM NaCl, and 2.7 mM KCl) containing 1.0 μM CP1 solution for 2 h at room temperature, rinsed with copious amount of DI water, and dried in a stream of nitrogen. At this stage, one could expect self-assembled monolayers (SAM) of CP1 on both electrodes (top and bottom) through thiol−gold interaction. Subsequently, the device was subjected to electrochemical stripping that would selectively and completely remove CP1 from the bottom electrode. A single potential cycling of the bottom electrode was performed between 0 and 1.0 V (vs Ag/AgCl) at a scan rate of 200 mV/s. Next, the device was incubated in a solution containing 1.0 μM CP2 for 2 h at room temperature. It was ready after a thorough wash with DI water.

Hybridization and Detection. After immobilization of CP1 and CP2 on the two electrodes, respectively, the nanogap was bridged by a 30 min hybridization with aliquots of 5.0 μL of the target DNA of various concentrations in TE buffer (10 mM Tris-HCl at pH 8.0, 100 mM NaCl, and 1.0 mM EDTA) where the two termini were complementary to the two surface-bound capture probes, respectively. After hybridization, the device underwent three stringency washes with SSC buffer (80 mM NaCl, 8 mM sodium citrate, and 0.1% sodium dodecyl sulfate; 5−7 °C below melting temperature) to remove any nonspecifically adsorbed or partially hybridized DNA strands. Finally, the hybridized molecules across the gap were made electrically conducting by a simple metallization step. The process consists of the vectorial "collection" of silver ions along the hybridized DNA strands followed by hydroquinone-catalyzed reductive formation of silver nanowires along the DNA skeletons.[25] Briefly, the hybridized sensor was incubated in 0.10 M $AgNO_3$ in ammonia (pH = 10.5) for 10 min. After a thorough rinsing, the adsorbed silver ions were reduced by 50 mM hydroquinone in ammonia (pH = 10.5). The conductance measurements were performed with a parameter analyzer. To better visualize the formation of silver nanowires, a silver enhancement process was applied to the samples for scanning electron microscopic (SEM) experiments. That is, after the silver ion collection and reduction on the sensor, 1.0 mM $AgNO_3$ in citrate buffer (pH = 3.5) and 2.0 mM hydroquinone in citrate buffer (pH = 3.5) were mixed and applied onto the sensor. Usually 5−10 min was sufficient to form highly visible silver nanowires under SEM.

Results and Discussion

Nano-MIM Device Fabrication. Illustrations of the nanogap device along with the sensing procedure are depicted in Figure 2. The nano-MIM was fabricated, where a nanometer-thick layer of SiO_2 (insulator) was sandwiched between a pair of vertically stacked metal layers (conductors). The SiO_2 insulating layer forms a "nanogap" between the top and the bottom metal electrodes on which two capture probes with different sequences, complementary to the two termini of the target DNA, respectively, were immobilized. Bridging of this nanogap by the target DNA strand, upon hybridization and subsequent silver nanowire formation, creates a primary current pathway (Figure 2B). Noncomplementary DNA strands, that fail to hybridize with the capture probes, do not bridge across the insulator layer and thus will not contribute to the current between the two metal electrodes. Vital to the feasibility of this approach is to have a

(25) Braun, E.; Eichen, Y.; Sivan, U. *Nature* **1998**, *391*, 775–778.

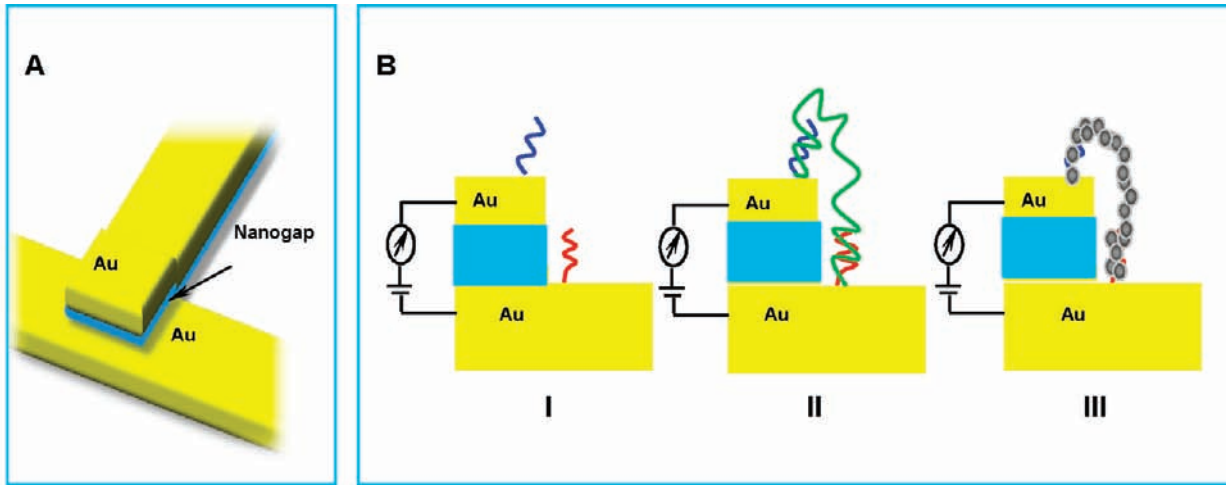

Figure 2. (A) Schematic illustration of the nano-MIM sensor device. A 5−20 nm thick insulating layer is sandwiched between a pair of Au microelectrodes. The width of the nanogap can easily be modulated by changing the insulating layer thickness. (B) Sensing procedure: (I) two different capture probes immobilization across the nanogap; (II) hybridization with target DNA (green); (III) formation of silver wires along the backbone of the bridging molecule that results in formation of an electrical conducting pathway(s) between the electrode pair.

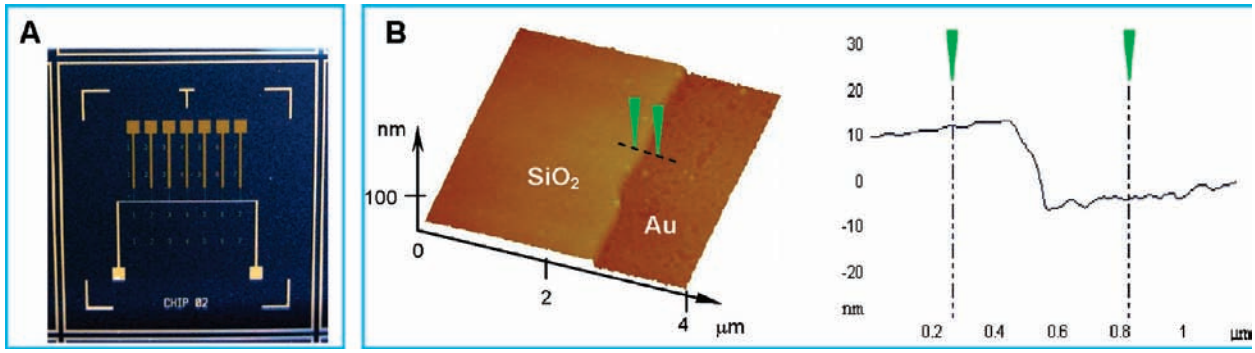

Figure 3. (A) Stereomicroscopic image of a typical nanogap sensor array chip (dimension: 10 mm × 10 mm). (B) Atomic force microscopy (AFM) image of the insulator/bottom electrode interface.

nominal background current, which should preferably be several orders of magnitude lower than the signal generated after DNA bridging. In general, the background current is primarily due to tunneling of charge carriers through the SiO_2 insulating layer in the relatively large common area of the electrodes (5 μm × 5 μm). For demonstration purpose, an array of seven devices was fabricated on a 100 mm^2 substrate area (Figure 3A), although a higher scale of integration is possible following the same fabrication procedure. By using this process, we have fabricated the nanogap sensor arrays of different gap sizes that varies from 5 to 100 nm with precise control of gap size (±1.0 nm) with high device uniformity and unlimited scalability. As we know, the morphology and electrical properties of the SiO_2 insulating layer are critical for desired performances of the nano-MIM devices. For the 10−20 nm thick SiO_2 layer, surface roughness was found to be ~0.5 nm (Figure 3B). The leakage current (the conductance of the blank sensor chip) was found to be in the range 0.2−0.8 pS. This extremely low leakage current prompted subsequent applications of this device in DNA detection.

Capture Probes Immobilization. Now, each one set of the capture probes had to be selectively immobilized on one of the two corresponding electrodes across the nanogap (Figure 4A). In other words, a 10−20 nm resolution of the capture probe immobilization procedure is needed. This step was very critical because it is practically impossible to directly apply the capture probe solution on a particular electrode, even with the help of a robotic spotter. Fortunately, such a task was successfully accomplished by an electrochemical stripping technique developed in our lab during the course of this work. To provide direct evidence, we chose a few representative devices and incubated them in TE buffer containing 1.0 μM fluorophore-labeled target DNAs after each step. Referring to the fluorescence image in Figure 4B, it is apparent that CP1 indeed formed excellent SAMs on the surfaces of both electrodes. To verify the selective removal of CP1, after the electrochemical stripping, the devices were incubated with the Cy3-labeled complementary target and examined under a fluorescence microscope. As shown in Figure 4C, CP1 was only present on the top electrode of the nano-MIM device, judging from the complete disappearance of the fluorescence at the bottom electrode. Since a monolayer of CP1 was already present on the top electrode, the latter treatment with CP2 solution would presumably result in the formation of a SAM of CP2 on the bottom electrode. This was corroborated by incubating a set of the devices in the TE buffer solution containing 1.0 μM of FAM (green dye)-labeled target DNA with its base sequence complementary to CP2 and the Cy3-labeled DNA with its base sequence complementary to CP1. Figure 4D provides an excellent visual proof that we were very successful in selectively immobilizing SAMs of two different capture probes on the surfaces of a pair of nanometer-spaced electrodes. This is the first time that nanometer resolution in DNA immobilization was achieved. In addition, the fluorescence images strongly suggest a high surface coverage of the im-

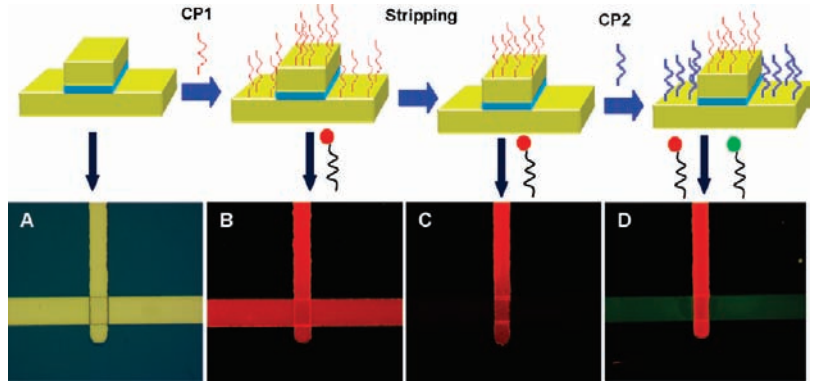

Figure 4. Immobilization of two different capture probes on the two electrodes separated by a nanometer gap: (A) optical image of a cleaned MIM device; (B) fluorescence image of the device after immobilization of CP1 and hybridization with its complementary target DNA tagged with Cy3 dye; (C) electrochemical stripping of CP1 from the bottom electrode followed by hybridization with the Cy3-labeled DNA; (D) fluorescence image after immobilization of CP2 and hybridization with respective complementary DNAs tagged with Cy3 and FAM dyes.

mobilized capture probes and an excellent hybridization efficiency, which paves the way for the development of ultrasensitive DNA sensing devices. Moreover, nonspecific adsorption on the substrate or the electrode surface was negligible as is evident from the very clean fluorescence images.

Detection of Target DNA. Two terminal electrical measurements were made across the pair of the nanogapped electrodes in each nano-MIM device. Figure 5A depicts a typical current−voltage ($i-V$) characteristic curve for a sample solution containing 1.0 fM target DNA, as referred to that for the background (control). At a bias voltage of 1.0 V, about 2 orders of magnitude higher current could be detected for the devices after hybridization and silver metallization. The representative curve is nonlinear, which is likely to be caused by intergrain boundary resistance in the silver nanowire.[26,27] Devices in an array that underwent identical treatments yielded similar $i-V$ curves.

To verify the authenticity of the response, we conducted a series of control experiments. First, we replaced CP1 with another capture probe (CP*) of the same length but having five central bases noncomplementary to the corresponding terminal of PKB2. The hybridization, washing, and silver metallization conditions were all kept unchanged. No noticeable change in the background current could be observed, strongly indicating that the noncomplementarities introduced into the system precludes the target DNA to completely hybridize with CP* and hence unable to withstand the stringency washes. DNA strands that do not hybridize with the capture probes at the top electrode will probably lie flat at the bottom electrode, having no contribution to the conductance of the device at all. We also spotted a droplet of blank buffer solution, and the device underwent exactly the same procedure. Again, no detectable signal was observed, confirming that output current did not originate from accidental bridging of the nanogap due to uncontrolled enhancement of the silver seeds formed along the capture probes. Finally, we verified if the nonspecific adsorption of the long target DNA, for example PKB2, across the nanogap could contribute to the signal. For this test, we incubated several freshly cleaned devices, preimmobilized with noncomplementary capture probes, with the target DNA solution and then followed the optimized silver ion collection and nanowire formation

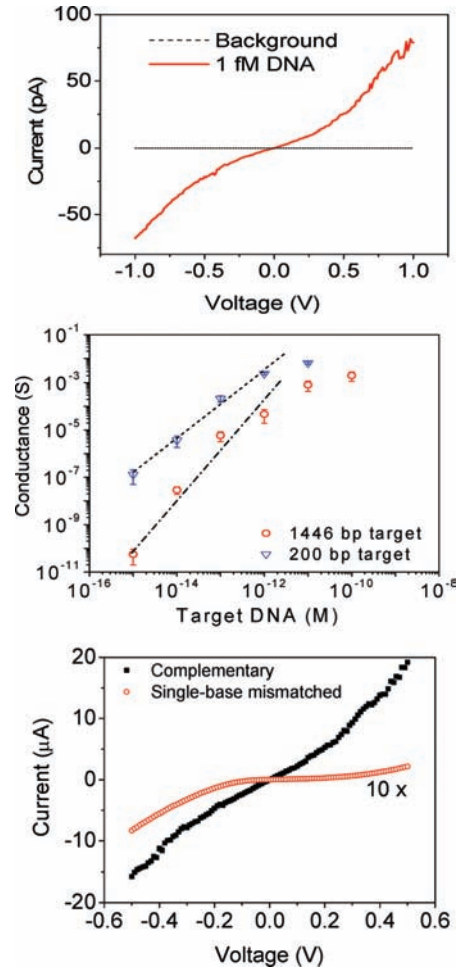

Figure 5. (A, top) Representative $i-V$ curve for 1.0 fM target DNA as referred to background (control) and (B, middle) calibration curves, and (C, bottom) $i-V$ curves of mismatch discrimination tests at 1.0 pM. For clarity, the $i-V$ curve of the single-base mismatched target is scaled up 10 times. The error bars represent the variation of data for each set of five measurements.

procedures. The absence of any detectable change in conductance further confirmed the reliability of the measured signals.

Utilizing this hybridized DNA-templated formation of silver nanowires as the signal generator, the conductance between the nanogapped electrodes is primarily dependent on the number of the silver nanowires formed between the top and the bottom

(26) Green, N. G.; Morgan, H. *J. Phys. D: Appl. Phys.* **1997**, *30*, L41–44.
(27) Heinzel, T. *Mesoscopic Electronics in Solid State Nanostructures*; Wiley-VCH: Weinheim, Germany, 2003; p 225.

electrode (bridging). The more the target DNA molecules hybridized, the more the silver nanowires are expected between the two electrodes, thus the higher is the conductance. Under controlled experimental conditions, a simple and straightforward linear relationship between the conductance and the target DNA concentration can be expected. To construct the calibration curve, multiple measurements were carried out for each concentration to obtain the average of the conductance. Indeed, as shown in Figure 5B and Figure S3 of the Supporting Information, conductance between the electrode pair was found to increase with an increase in target DNA concentration. We correlate this concentration-dependent conductance to the statistical number of silver nanowires formed between the electrode pair. In the case of ultralow DNA concentration (e.g., 1.0 fM), only a few copies can potentially hybridize and bridge up the nanogap. As the concentration of target DNA in the test solution increases, more DNA strands hybridize across the gap, which in turn enhances the number of parallel conduction pathways. Under optimized conditions, the target DNA can be quantitatively detected in a dynamic range from 1.0 fM to 1.0 pM with a total analysis time from hybridization to detection well within 60 min per sensor chip. This sensitivity is comparable to the best of electrochemical/electrical biosensors.[9,28−31] The regression coefficient R^2 and the relative standard derivation (RSD) were found to be 0.96 and ≤20%, respectively. Such signal variations reflect the cumulative degree of reproducibility of the capture probe immobilization, hybridization, silver ion collection, and nanowire formation steps. Slightly lower detection limits of 0.3−0.5 fM, depending on the length of the gene (the shorter ones were more sensitive probably due to higher hybridization efficiency), were achievable after a much prolonged hybridization of 4−6 h but with little practical significance in view of the long hybridization time. As seen in Figure 5B, at the high concentration end of the calibration curve, the conductance reached as high as millisiemens, 1.25×10^9 times higher than the background, which translates into a relative change of 2.1×10^4% per unit concentration, which is far better than any other electrical transduction-based methods.[28−31] This huge signal intensity is mainly due to a significantly reduced background conductance (<1.0 pS) achieved with the vertical nanogap since other nano- and microgapped electrodes can also produce a conductance at millisiemens levels but on a huge background of submicrosiemens.[28−31] Unlike planar nano- and microstructures where all target DNA molecules, hybridized, loosely bound, and nonspecifically adsorbed, contribute to the conductance of the device,[28,30] the extremely low background suggests that the unique vertical nano-MIM structure and the two-capture probe approach significantly reduce the background to a level comparable to the instrument noise in DNA detection, since bridging is attained only when both termini of the target DNA hybridize with the capture probes. In other words, to generate a conductance increment, the target DNA molecule must be "held" vertically by the two capture probes across the nanogap. Target DNA strands found lying at the bottom electrode have very little effect on the conductance. In principle, detections of target DNA strands ≥60 base pairs can be performed at 10 nm nanogap sensor arrays, which cover almost all known genes.[32]

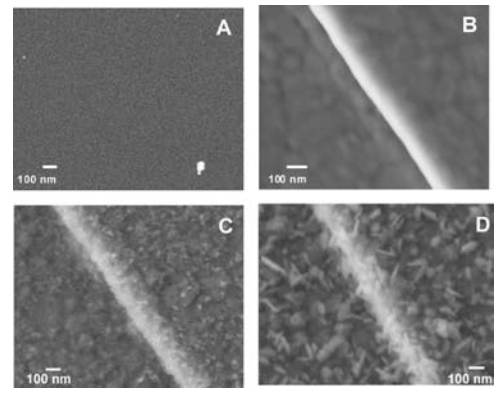

Figure 6. SEM images: (A) silicon oxide after silver treatment; (B) a blank sensor chip at the nanogap junction; (C) a capture probe coated control sensor chip; (D) a 1.0 pM PKB2 hybridized sensor chip after silver treatment.

To evaluate the capability of the proposed procedure in discriminating single-base-mismatch (SBM), CP1 was substituted with capture probes of the same length but having only one A−T mismatch in the middle, so that the new devices were single-base-mismatched to the same target DNA. At 1.0 pM, it was found that the conductance increments for the SBM devices were <4% of those found with the fully complementary ones (Figure 5C). That is to say, the detection of the SBM mutations is possible with the proposed procedure with a SBM selectivity factor of at least 25:1, much higher than that of the optical microarray and most other previously reported methods.[28,30] Again, this is probably due to the vertical configuration of the nanogap, which practically eliminates most of the nonhybridization-related contributions (background). Assuming the background remains unchanged under all circumstances, its contribution to the SBM selectivity can be described as

$$\text{Background contribution} = (S_{\text{comp}} + B)/(S_{\text{SBM}} + B) - (S_{\text{comp}}/S_{\text{SBM}}) \quad (1)$$

where S_{SBM}, B, and S_{comp} are the conductances of SBM DNA, background, and the complementary DNA, respectively. As $S_{\text{comp}} > S_{\text{SBM}}$ and $B < S_{\text{SBM}}$,

$$\text{Background contribution} = B(S_{\text{SBM}} - S_{\text{comp}})/(S_{\text{SBM}}(S_{\text{SBM}} + B)) < 0 \quad (2)$$

As seen in eq 2, the background contribution to the SBM selectivity is always negative. With a high background, a significant amount of the mismatch selectivity is lost. The true SBM selectivity of hybridization-based DNA sensors can only be realized when the background is negligible.

SEM characterization was then performed on the biosensor chips exposed to the control and to the complementary DNA samples. The images are shown in Figure 6. It is seen that the silicon oxide surface of the sensor chip showed no visible change before and after silver deposition (Figure 6A), while after silver nanowire deposition, the capture probe coated gold electrodes were obviously roughened by the presence of the silver nanowire, or rather nanoparticles, which were supposed to be

(28) Rosi, N. L.; Mirkin, C. A. *Chem. Rev.* **2005**, *105*, 1547–1562.
(29) Liu, G.; Wan, Y.; Gau, V.; Zhang, J.; Wang, L. H.; Song, S. P.; Fan, C. H. *J. Am. Chem. Soc.* **2008**, *130*, 6820–6825.
(30) Fan, Y.; Chen, X. T.; Trigg, A. D.; Tung, C. H.; Kong, J. M.; Gao, Z. Q. *J. Am. Chem. Soc.* **2007**, *129*, 5437–5443.
(31) Moller, R.; Powell, R. D.; Hainfeld, J. F.; Fritzsche, W. *Nano Lett.* **2005**, *5*, 1475–1482.
(32) Gonzalez-Pastor, J. E.; Millan, J. L. S.; Moreno, F. *Nature* **1994**, *369*, 281.

the agglomeration of the short nanowires (Figure 6C). For comparison, the SEM image of a blank sensor chip is represented as Figure 6B. One possible reason may be the densely packed short capture probes (6−7 nm), which will inevitably aggregate with the growth of the silver nanowires. Another possible reason may be that the overwound polymorph and agglomeration of the silver nanowires occurred with the concomitant shielding of the negative charges on the capture probes with the proceeding of the silver nanowire formation, reducing the electrostatic repulsion between adjacent capture probes.[33,34] The capture probes are supposed to "stand" on the gold surface due to electrostatic repulsion between adjacent strands. The shielding of the negative charges with the proceeding of silver formation leads to the aggregation of the DNA−silver adducts. The capture probes no longer stand on but bend down to the gold surface. Therefore, the deposited silver was likely to take on an uneven agglomerated netlike configuration other than independent wires with clear boundaries. Fortunately, agglomeration is a desirable feature in developing an electrical detection procedure with the vertically aligned nanogap electrodes because it facilities the formation of two-dimensional features on the electrode surface instead of three-dimensional features toward the top electrode, largely reducing the possibility of nanogap bridging by the capture probes and making it possible to read electrical signal with high signal-to-noise ratio. The morphology of the silver deposited at the control is distinctly different from the wirelike silver deposited at the complementary DNA hybridized sensor surface under identical conditions (Figure 6D). A close examination of Figure 6D revealed that, indeed, there are some silver nanowires vertically aligned across the nanogap, effectively bridging the two gold electrodes, generating a measurable electrical signal.

(33) Nagarijan, R.; Roy, S.; Kunar, J.; Tripathy, S. K.; Dolukhanyan, T.; Sung, C.; Bruno, F.; Samuelson, L. A. *J. Macromol. Sci., Pure Appl. Chem.* **2001**, *A38*, 1519–1537.

(34) Akkara, J. A.; Senecal, K. J.; Kaplan, D. L. *J. Polym. Sci., Part A: Polym. Chem.* **1991**, *29*, 1561–1574.

Conclusion

In conclusion, we have demonstrated a novel ultrasensitive sensor array for the detection of DNA with a femtomolar detection limit after a 30 min hybridization. This sensitivity is among the best of electrical DNA biosensors. We proposed a fabrication technique of the nano-MIM sensor array that can be mass produced using conventional, high-yield fabrication processes. Because of the extremely low background, exceptional signal intensity and excellent mismatch discrimination were obtained. Following the present process steps, the sensor array can be integrated on a readout unit for detecting a range of target DNAs. The sensor arrays detailed in this work can be especially beneficial where rapid, parallel DNA analysis is needed (e.g., for characterizing pathogens, measuring mRNA levels during expression profiling, or point-of-care applications).

Acknowledgment. This work was funded by the Institute of Bioengineering and Nanotechnology (Biomedical Research Council, Agency for Science, Technology and Research, Singapore).

Supporting Information Available: Ellipsometric study of the silicon oxide film, DNA sequence information, AFM images of the sensor chip, and $i-V$ curves of target DNA at different concentrations. This material is available free of charge via the Internet at http://pubs.acs.org.

JA901704T